Journal of Molecular Catalysis A: Chemical 313 (2009) 107–113

Contents lists available at ScienceDirect

Journal of Molecular Catalysis A: Chemical

journal homepage: www.elsevier.com/locate/molcata

Effects of urea on the microstructure and photocatalytic activity of bimodal mesoporous titania microspheres

Minghua Zhou[a,b,1], Jiaguo Yu[a,*], Huogen Yu[a,1]

[a] State Key Laboratory of Advanced Technology for Material Synthesis and Processing, Wuhan University of Technology, Luoshi Road 122, Wuhan 430070, PR China
[b] Staff Room of Chemistry, Yunyang Medical College, Shiyan 442000, Hubei, PR China

ARTICLE INFO

Article history:
Received 20 April 2009
Received in revised form 9 June 2009
Accepted 13 August 2009
Available online 21 August 2009

Keywords:
Mesoporous
TiO_2 microspheres
Bimodal
Photocatalytic activity
Hydrothermal
Hydroxyl radicals

ABSTRACT

Bimodal mesoporous TiO_2 microspheres with high photocatalytic activity were prepared by a hydrothermal method using titanium sulfate as precursor in the presence of urea. The results indicate that all prepared samples show bimodal pore-size distributions in the mesoporous region: smaller intra-aggregated pores with peak pore diameter of ca. 2 nm and larger inter-aggregated pores with peak pore diameter of ca. 12.5 nm. The molar ratio of urea to $Ti(SO_4)_2$ (R_u) has an obvious influence on the morphology, microstructure and photocatalytic activity of TiO_2. With increasing R_u, specific surface areas and porosity increase, contrarily, the crystallite size and relative anatase crystallinity decrease. The photocatalytic activity first increases with R_u. At $R_u = 2.0$, the photocatalytic activity reaches the highest and is obviously higher than that of Degussa P25. With further increasing R_u, the photocatalytic activity decreases. The formation rate of hydroxyl radicals during photocatalysis has a positive correlation with the photocatalytic activity.

1. Introduction

Titania is a very important multifunctional environment and energy material because of its peculiar and fascinating physicochemical properties and a wide variety of potential uses in diverse fields including solar energy conversion, environmental purification, and waste water treatment [1–5]. Although titania powders and sols can be readily prepared by conventional precipitation or sol–gel methods, synthetic routes to mesoporous TiO_2 spheres with good crystallization, small crystallite size and high specific surface area and pore volume are less common. Also, the mesoporous TiO_2 microspheres obtained by conventional template methods are amorphous in nature and high-temperature calcination (higher than 400 °C) is required to realize the phase transformation from amorphous to anatase and to remove the organic templates. Thus, such a high-temperature will cause the obvious growth of crystallites, resulting in the decrease of specific surface areas and the destruction of pore structure [4–7]. Therefore, in order to obtain highly photoactive mesoporous TiO_2 microspheres with good crystallization, small crystallite size and high specific surface area and pore volume, an optimal method is to realize the phase transformation of amorphous to anatase at low temperatures in the absence of templates or surfactants.

Soler-Illia et al. [8,9] have in detail reported the urea method as an efficient route to synthesize both amorphous and crystalline metal (hydrous) oxide with uniform particle shape from an aqueous media. The decomposition of urea in aqueous solution is accompanied by slow and controlled supply of ammonia and carbon dioxide into solution. The smooth pH increase obtained by the decomposition of urea in synchrony with the active release of OH^- and CO_3^{2-} ions, usually leads to the precipitation of metal hydrous oxide particles of controlled particle morphology. However, to the best of our knowledge, there are few papers on the preparation and photocatalytic activity of bimodal mesoporous TiO_2 microspheres for the photocatalytic decomposition of acetone in air. Herein, we adopt a simple one-step template-free hydrothermal method to synthesize bimodal mesoporous TiO_2 microspheres by using urea and $Ti(SO_4)_2$ as precursors at 160 °C. Urea is used as a dual-function agent, as a pore-produced agent and pH adjusting agent. The preparation conditions are much milder and simpler than those of the conventional template methods, which require high-temperature calcination procedures. Another advantage is that the as-prepared samples show bimodal mesoporous structure, which will endow them with better mass transport for reactant molecules and larger light-harvesting ability due to hierarchically porous structures, resulting in an enhanced photocatalytic activity.

* Corresponding author. Tel.: +86 27 87871029; fax: +86 27 87879468.
E-mail address: jiaguoyu@yahoo.com (J. Yu).
[1] Tel.: +86 27 87871029; fax: +86 27 87879468.

1381-1169/$ – see front matter © 2009 Elsevier B.V. All rights reserved.
doi:10.1016/j.molcata.2009.08.009

2. Experimental

2.1. Synthesis

All the chemicals used in this study were reagent-grade and deionized water was used in the whole experiment. The bimodal mesoporous TiO_2 microspheres were synthesized by hydrothermal treatment of $Ti(SO_4)_2$ in a $CO(NH_2)_2$ aqueous solution. The molar ratio of $CO(NH_2)_2$ to $Ti(SO_4)_2$ (R_u) was varied from 0, 1, 2, 4 to 8. After continuous stirring for 30 min, the mixed solution was transferred into a Teflon lined stainless steel autoclave. Before hydrothermal reactions, the pH values of all the mixed solutions were about 1.0. The autoclave was incubated at 160 °C for 5 h and then cooled to room temperature. After hydrothermal reaction, the pH values of the corresponding mixed solution changed greatly and were about 0.5, 2.0, 4.5 6.5 and 8.8, respectively. The white precipitates were centrifuged, and washed with distilled water and alcohol for five times. The washed precipitates were dried in a vacuum oven at 80 °C for 12 h.

2.2. Characterization

X-ray diffraction (XRD) patterns obtained on a D/Max-RB X-ray diffractometer (Rigaku, Japan) using Cu Kα irradiation at a scan rate (2θ) of 0.05° s^{-1} were used to determine the phase structure of the obtained samples [10,11]. Morphology observation was performed on an S-4800 field emission scanning electron microscope (SEM, Hitachi, Japan). Transmission electron microscopy (TEM) and high-resolution transmission electron microscopy (HRTEM) observation were conducted using a JEM 2100F microscope. The Brunauer–Emmett–Teller surface areas (S_{BET}) of the samples were analyzed by nitrogen adsorption with a Micromeritics ASAP 2020 nitrogen adsorption apparatus (USA).

2.3. Analysis of hydroxyl radical (•OH)

The formation of hydroxyl radical (•OH) on the surface of photo-illuminated TiO_2 was detected by photoluminescence (PL) technique using terephthalic acid as a probe molecule [12,13]. This method relies on the PL signal at 425 nm of the hydroxylation of terephthalic acid with •OH generated at the TiO_2/water interface. Furthermore, this method is rapid, sensitive and specific, and needs only a simple standard PL instrumentation. Experimental procedures are as follows: 0.10 g of the TiO_2 sample was dispersed in a 25 mL of the 5×10^{-4} M terephthalic acid aqueous solution with a concentration of 2×10^{-3} M NaOH in a dish with a diameter of about 9.0 cm. A 15 W, 365 nm UV-lamp was used as a light source. PL spectra of generated 2-hydroxyterephthalic acid were measured on a Fluorescence Spectrophotometer (F-7000, Hitachi, Japan).

2.4. Measurement of photocatalytic activity

In this work, we chose acetone as a model compound to evaluate the photocatalytic activity of the as-prepared samples. Photocatalytic oxidation of acetone is based on the following reaction [14–16]:

$$CH_3COCH_3 + 4O_2 \rightarrow 3CO_2 + 3H_2O \quad (1)$$

The weight of catalysts used for each experiment was kept at 0.20 g and coated onto three dishes. After TiO_2-coated dishes were placed in the reactor, a 15 ± 1 μL acetone was injected into the reactor with a microsyringe. The analysis of acetone, carbon dioxide, and water vapor concentration in the reactor was on-line conducted with a Photoacoustic Field Gas-Monitor (INNOVA Air Tech Instruments Model 1412). The acetone vapor was allowed to reach adsorption equilibrium with catalysts in the reactor prior to UV light irradiation. The initial concentration of acetone after adsorption equilibrium was controlled at 300 ± 20 ppm, which remained constant for about 5 min until a 15 W, 365 nm, UV-lamp in the reactor was turned on. The initial temperature was 25 ± 1 °C and each set of experiment under UV irradiation was performed for 60 min. The photocatalytic activity of the samples can be quantitatively evaluated by comparing the removal efficiency of acetone (R(%)). R(%) was calculated according to the following equation [10]:

$$R(\%) = \frac{c_0 - c_t}{c_0} \times 100\% \quad (2)$$

where c_0 and c_t represent the initial equilibrium and reaction concentration of acetone, respectively.

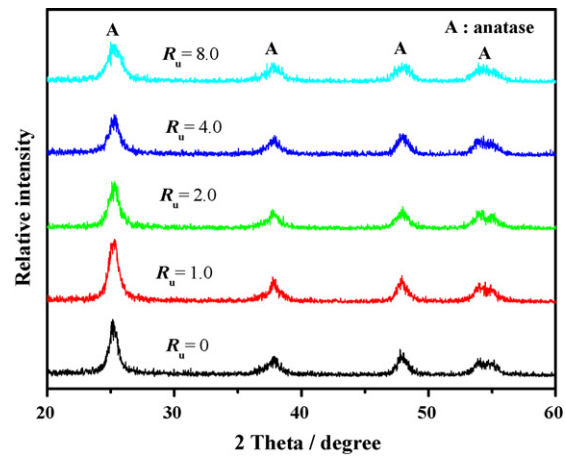

Fig. 1. XRD patterns of the TiO_2 samples prepared at different R_u.

3. Results and discussion

3.1. Crystal structure

Fig. 1 shows XRD patterns of the TiO_2 samples prepared at different R_u. The diffraction peaks of all samples are easily indexed to the anatase phase of TiO_2, which is consistent with the pure anatase phase of TiO_2 (space group: $I4_1/amd$ (1 4 1); JPCDS No. 21-1272) [17,18]. Usually, the phase transformation temperature from amorphous to anatase is higher than 400 °C in air. It can be concluded that hydrothermal treatment can promote the phase transformation from amorphous to anatase at a low temperature (160 °C). Further observations indicate that, with increasing R_u, the peak intensities of anatase become weaker and the width of the diffraction peaks of anatase show slightly wider, indicating the formation of smaller TiO_2 crystallites. The relative anatase crystallinity is quantitatively evaluated via the relative intensity of the (1 0 1) diffraction peak [19]. Table 1 lists the average crystalline sizes and relative anatase crystallinity of TiO_2 samples prepared at different R_u. It can be seen that the average crystalline sizes and relative anatase crystallinity decrease with increasing R_u. This is attributed to the fact that, in pure water, the preparation of anatase TiO_2 powders from the inorganic salt precursor $Ti(SO_4)_2$ may undergo the following three consecutive reaction processes via hydrothermal method [20,21]:

$$Ti(SO_4)_2 + 4H_2O \rightarrow Ti(OH)_4 + 2H_2SO_4 \quad \text{Hydrolysis} \quad (3)$$

$$Ti(OH)_4 \rightarrow TiO_2(\text{amorphous}) + 2H_2O \quad \text{Condensation} \quad (4)$$

$$TiO_2(\text{amorphous}) \rightarrow TiO_2(\text{anatase}) \quad \text{Crystallization} \quad (5)$$

Clearly, the pH value greatly affects above hydrolysis and condensation reactions. In general, Eq. (3) is a rate-determining step of above three reactions and its rate is much slower at acid conditions,

Table 1
Effects of R_u on physical properties of bimodal mesoporous TiO_2 microspheres.

R_u	[a]Phase	S_{BET} (m^2/g)	Pore volume (cm^3/g)	Average pore size (nm)	Porosity (%)	[b]Crystallite size (nm)
0	A	152.8	0.36	13.2	58.1	13.2 (1.0)
1.0	A	166.6	0.39	12.4	60.0	11.3 (0.97)
2.0	A	179.0	0.43	11.9	62.3	10.6 (0.78)
4.0	A	195.9	0.49	11.5	65.3	8.6 (0.72)
8.0	A	215.9	0.55	11.2	67.9	7.6 (0.54)
P25	A + R	63.0	0.06	3.8	18.6	30.0 (A)

[a] A and R denoted anatase and rutile, respectively.
[b] Relative anatase crystallinity: the relative intensity of the diffraction peak from the anatase (1 0 1) plane (indicated in parentheses, reference: $R_u = 0$).

and can be rapidly enhanced at a basic environment. Therefore, in the absence of urea, the hydrolysis of $Ti(SO_4)_2$ in pure water can cause the production of H_2SO_4. Under such strong acid condition (pH = 0.5), the rate of hydrolysis and condensation reactions is rather slow and the nucleation is suppressed. So, fewer metastable tiny TiO_2 nanoclusters are formed. This is beneficial to crystal growth, rather than aggregation. The added urea has important influence on the rate of reaction (3) due to the following reactions [8,22–24]:

$$(NH_2)_2CO + 3H_2O \rightarrow 2NH_3{\cdot}H_2O + CO_2 \quad \text{Decomposition} \quad (6)$$

$$2NH_3{\cdot}H_2O + H_2SO_4 \rightarrow (NH_4)_2SO_4 + 2H_2O \quad \text{Neutralization} \quad (7)$$

The urea is decomposed into ammonia and carbon dioxide (Eq. (6)) at 160 °C and then the produced ammonia is neutralized by H_2SO_4 produced in Eq. (3) (Eq. (7)). According to the Le Chatelier's principle, reaction (3) is promoted due to the decrease of concentration of produced H_2SO_4 or the increase of pH value of the solution. Consequently, the rate of Eq. (4) is enhanced with increasing R_u. Thus, in hydrothermal conditions, the faster condensation rate will result in smaller crystalline sizes and weaker anatase crystallinity [25].

3.2. SEM and TEM studies

Fig. 2 shows the typical SEM images of the TiO_2 samples obtained at different R_u. As shown in Fig. 2a, the irregular aggregated

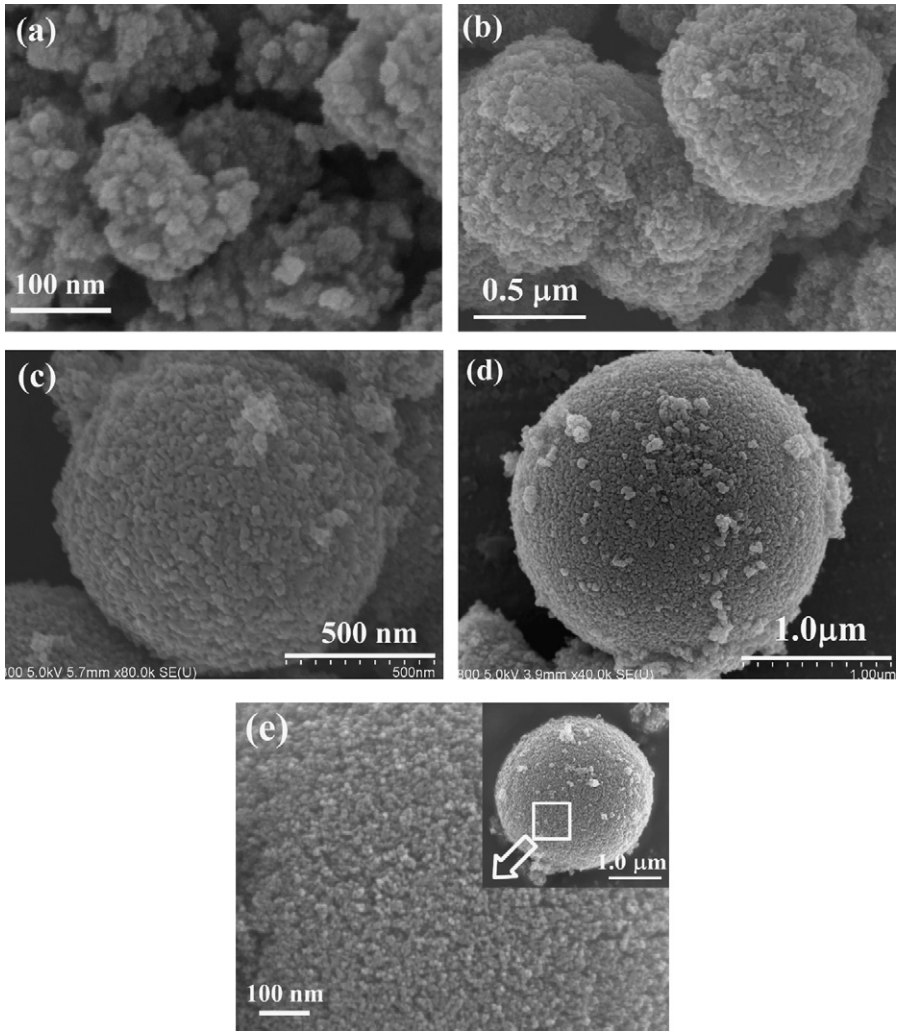

Fig. 2. SEM images of the samples prepared at different R_u. (a) $R_u = 0$, (b) $R_u = 1.0$, (c) $R_u = 2.0$, (d) $R_u = 4.0$ and (e) $R_u = 8.0$. Inset in (e) showing SEM images of corresponding single microsphere.

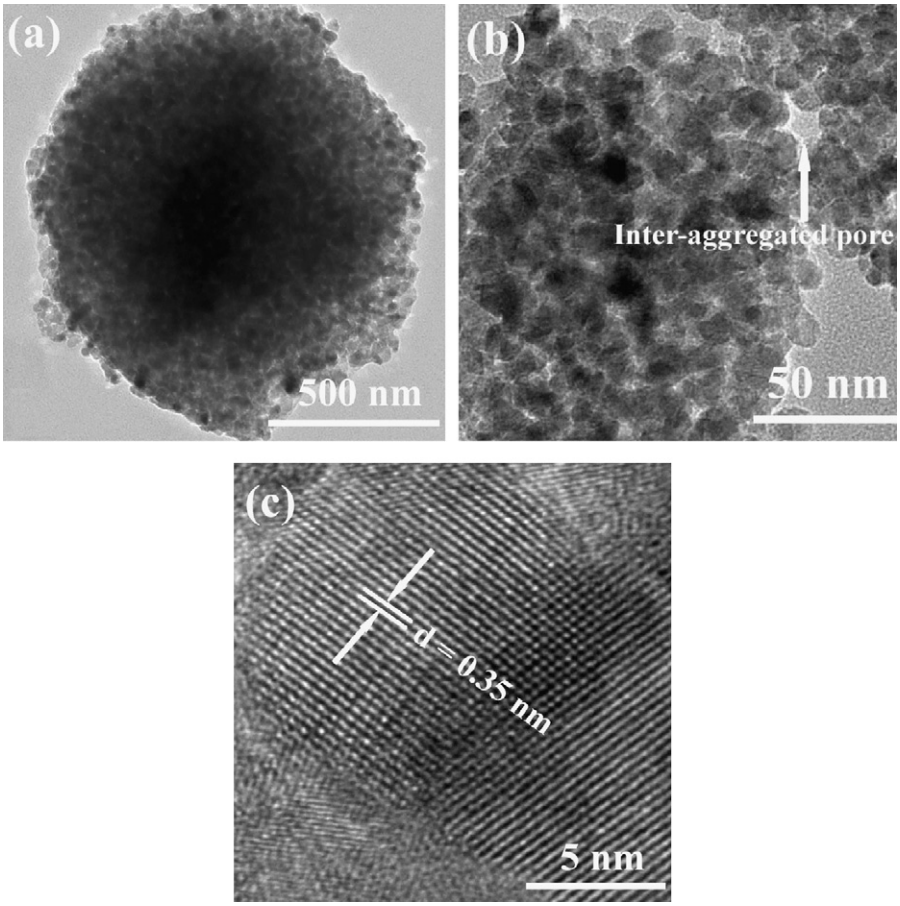

Fig. 3. TEM (a and b) and HRTEM (c) images of the bimodal mesoporous TiO_2 microspheres prepared at $R_u = 2.0$.

particles with rough surface are obtained in the absence of urea (in pure water, $R_u = 0$). Furthermore, the pH value of the mixture solution is about 0.5, which is much lower than that of the isoelectric points of TiO_2 (pH = 5.5–6) and thus each primary TiO_2 crystallite is positively charged at such a strong acid solution [26,27]. So, these small primary TiO_2 crystallites cannot aggregate spontaneously to large spherical aggregates because of their electrostatic repulsion. Taking the above XRD results into account, the amount of urea also plays an important role in controlling the morphology of the final products. Urea can influence the microstructures of the TiO_2 via altering the pH values of the reaction system. When urea is added into the reaction solution, the microstructures of the TiO_2 samples have an obvious change. With increasing urea concentration ($R_u = 1.0$), the shape of the particles approximately transforms into spherical aggregates. This is probably due to the fact that when the pH of the mixed solution is adjacent to the isoelectric point of TiO_2, the electrostatic repulsion from primary crystallite decreases. So, the primary crystallites spontaneously aggregate into large microspheres to minimize their surface Gibbs energy. The average diameters of the microspheres slowly increase, while the roughness of the surface of the samples gradually decreases (Fig. 2b). Interestingly, with further increasing urea concentration to some extent ($R_u = 2.0$), TiO_2 spherical particles are obtained in addition to a small fraction of ill-defined small particles (Fig. 2c). At $R_u = 8$, the particles show the round external configuration with average diameter of ca. 3 μm. The enlarged SEM images (Fig. 2e) of the microspheres surface clearly reveal that these spherical architectures are composed of numerous secondary particles with many nanoscale channels, and the average diameter of the secondary particles is ca. 30 nm. The configuration of spherical microstructures is further investigated by the corresponding TEM images (Fig. 3a and b).

The corresponding TEM and HRTEM images of the sample prepared at $R_u = 2.0$ are presented in Fig. 3, which further confirm that the microspheres ca. 1 μm in size (see Fig. 3a and b) consist of primary crystallites. It can be seen that the primary crystallite size is about 11 ± 1 nm (Fig. 3b), which is in agreement with the value of the crystallite size determined by XRD (10.6 nm) (as shown in Table 1). Further observation indicates that a large number of small mesopores (intra-aggregated pores) come from the aggregation of primary crystallites and larger inter-aggregated pores are from the aggregation of secondary particles (marked by arrow in Fig. 3b). Fig. 3(c) shows clear lattice fringes of primary crystallite (0.35 nm corresponding to the (1 0 1) crystallographic plane of anatase) of the same sample, which allows for the identification of crystallographic spacing and indicates good crystallization of the prepared anatase TiO_2 microspheres.

3.3. BET surface areas and pore distributions

Fig. 4(a) shows the nitrogen adsorption–desorption isotherms of the bimodal mesoporous TiO_2 samples prepared at different R_u. All the samples show the isotherms of type IV [25,28]. With increasing R_u, the hysteresis loops shift to a lower relative pressure region and the adsorbed volume increases, which indicates that the average pore size decreases and specific surface area increases. The corresponding pore-size distribution of the prepared TiO_2 samples is shown in Fig. 4(b). It is interesting to find that all the samples show bimodal pore-size distributions. In pure water ($R_u = 0$), the powders contain fine intra-aggregated pores with peak pore diameters of

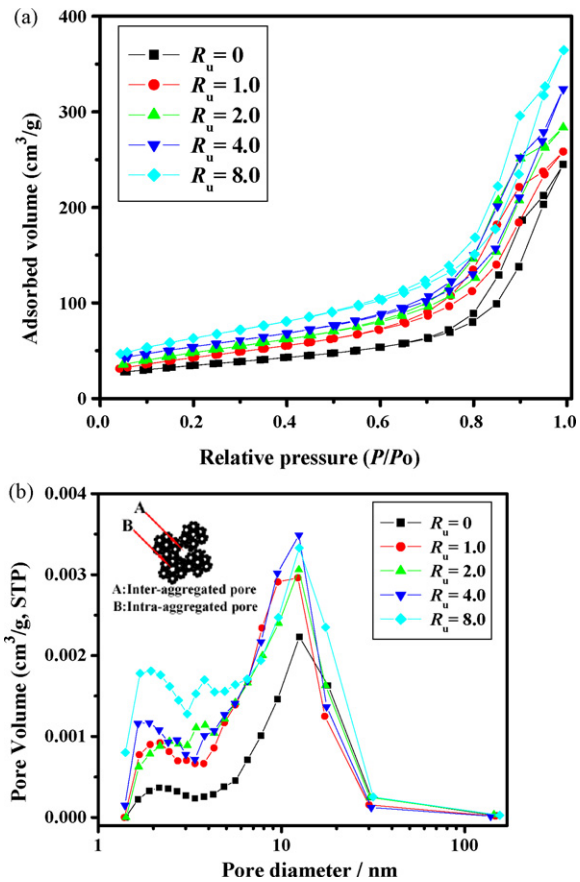

Fig. 4. Nitrogen adsorption–desorption isotherms (a) and corresponding pore-size distribution curves (b) of the bimodal mesoporous TiO_2 microshpheres prepared at different R_u.

ca. 2.1 nm and larger inter-aggregated pores with peak pore diameters of about 12.5 nm. According to our previous works [19], a bimodal pore-size distribution is due to two different aggregates in the powders. The smaller micro/meso-pores are usually related to primary intra-agglomeration (the hysteresis loop in the lower P/P_0 range), while the larger ones are associated with secondary inter-aggregation (the hysteresis loop in the higher P/P_0 range). It is these bimodal pores that can promote the rapid diffusion of various reactants and products during the photocatalytic reaction and enhance the rate of the photocatalytic reaction. With increasing urea concentration (R_u from 1.0 to 8.0), the peak pore sizes of the intra-aggregated pores shift into smaller meso/micropores regions (from 2.1 to 1.9 nm) and the inter-aggregated peak pore almost keeps un-change (12.5 nm), indicating the decrease of primary crystallite size. The quantitative details about the BET surface areas, pore volume, average pore size and porosity of the samples are presented in Table 1. It can be seen that with increasing R_u, the specific surface areas of the samples increase from 152.8 to 215.9 m^2/g and pore volume of the samples increase from 0.36 to 0.55 cm^3/g. While the average pore sizes decrease slightly from 13.2 to 11.2 nm.

3.4. Hydroxyl radical analysis

Terephthalic acid readily reacts with •OH to produce highly active fluorescent product, 2-hydroxyterephthalic acid [12,13]. This technique has been used in radiation chemistry, sonochemistry and biochemistry [29–36] for the detection of •OH generated in water. The intensity of the PL peak of 2-hydroxyterephtalic acid is proportional to the amount of •OH radicals produced at TiO_2/water interface [12,13]. Fig. 5 shows PL spectral changes with irradiation time. A gradual increase in PL intensity at wavelength range of 360–540 nm is observed with increasing irradiation time. Moreover, the generated spectra have the identical shape and peak position (at 425 nm).

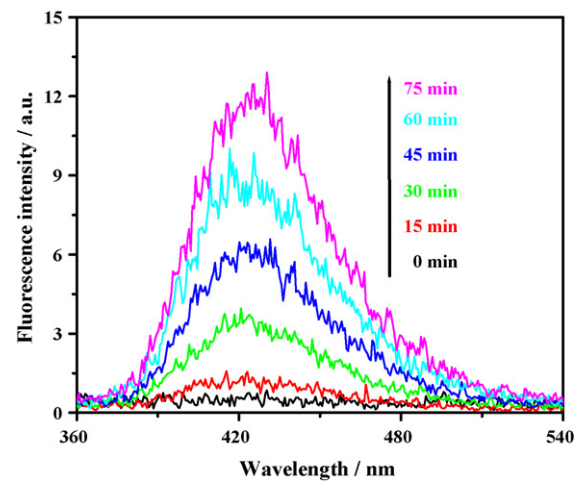

Fig. 5. PL spectral changes with irradiation time on the sample prepared at $R_u = 2.0$ in a 5×10^{-4} M basic solution of terephthalic acid.

Fig. 6 shows the plots of PL intensity at 425 nm against irradiation time. It can be seen that the PL intensity of terephthalic acid solutions under UV light irradiation increase linearly with time. Consequently, it can be reasonable to infer that the amount of •OH radicals produced at the TiO_2/water interface is proportional to the light irradiation time [12,13]. The formation rate of the •OH radicals can be expressed by the slop of these lines shown in Fig. 6. The order of the formation rate of •OH radicals formed on the surface of bimodal mesoporous TiO_2 microshpheres is as follows: $R_u = 2.0 > R_u = 4.0 > R_u = 1.0 > R_u = 0 > R_u = 8.0$, which suggests that the R_u influences the formation rate of •OH radicals and there is an optimal R_u.

3.5. Photocatalytic activity

Fig. 7 shows the concentration changes of acetone and carbon dioxide with time during photocatalytic reaction. It can be seen that the concentration of the produced carbon dioxide is about three

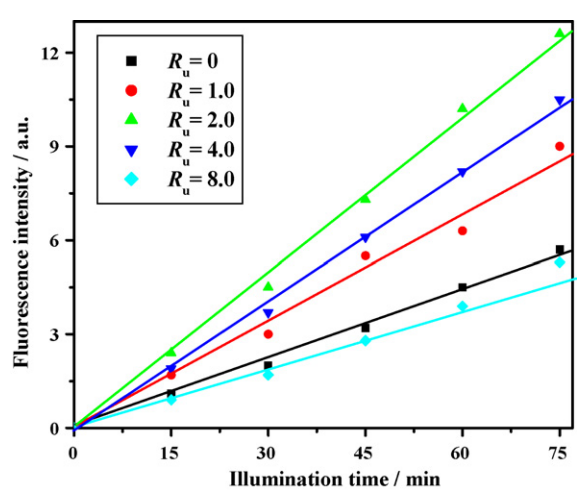

Fig. 6. Plots of the induced fluorescence intensity at 425 nm against irradiation time for terephthalic acid on the bimodal mesoporous TiO_2 microshpheres prepared at different R_u.

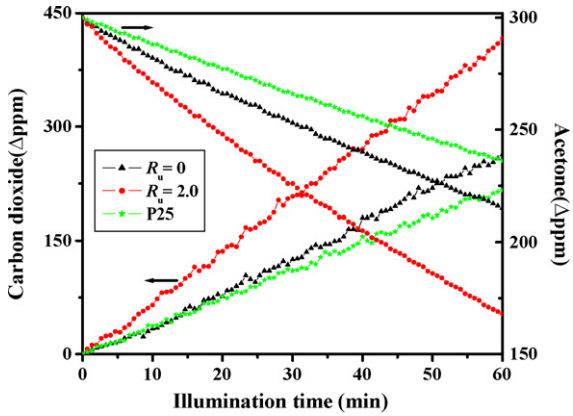

Fig. 7. Concentration–time plots of acetone and carbon dioxide (oxidation of acetone on the illuminated the samples prepared at R_u = 0 and 2.0 and P25).

times greater than the amount of the acetone destroyed. It is also observed that the concentration of the acetone and carbon dioxide linearly change with increasing irradiation time. Therefore, it can be concluded that the prepared photocatalysts and P25 can completely decompose acetone. Furthermore, the photocatalytic oxidation of acetone on the surface of TiO_2 powders in the initial time is also a pseudo-zero-order reaction, which is in agreement with the order of the formation rate of •OH radicals. Finally, the ascending sequence of photocatalytic activity of the samples is: P25 < R_u = 0 < R_u = 2.0 and the values of reaction kinetic constant are 1.07, 1.41 and 2.20 ppm/min for photocatalytic oxidation of acetone, respectively. In order to further characterize the performance of all photocatalysts, we also use R(%) to compare their photocatalytic activities.

Fig. 8 shows R(%) of acetone of all the samples prepared at different R_u. It can be seen that all the samples prepared by the hydrothermal method show better activities than P25. The higher photocatalytic activity of as-prepared microspheres may be first directly related to their bimodal mesoporous structures, which allows more efficient transport for the reactant molecules to get to the active sites on the framework walls, meanwhile, enhances the adsorption of light and reduce reflection of light, hence enhancing the efficiency of photocatalysis [37–44]. Of course, their large specific surface areas, pore volume and porosity are also beneficial to enhance their photocatalytic activity [45–47]. Further observation shows that R_u has an obvious influence on photocatalytic activity of the samples. At R_u = 0, the removal efficiency is 26.4%. With increasing R_u, the photocatalytic activity of the prepared samples increases slightly. At R_u = 2.0, the photocatalytic activity of the prepared sample reaches a maximum value, and its activity exceeds that of P25 by a factor of more than two times. With further increasing R_u, the photocatalytic activity of the prepared sample obviously decreases due to drastic decrease of relative anatase crystallinity.

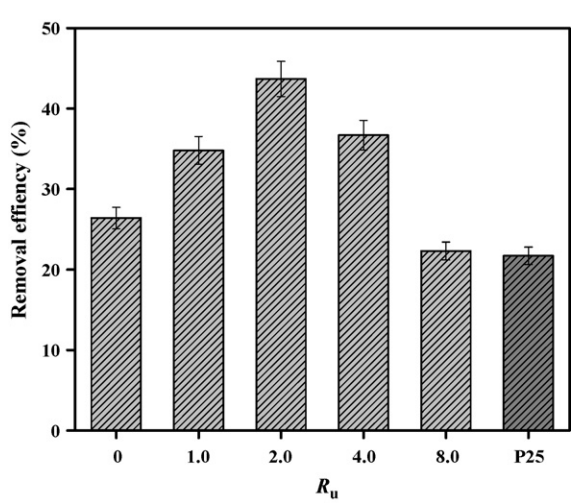

Fig. 8. The removal efficiency R(%) of acetone on the irradiated bimodal mesoporous TiO_2 microshpheres prepared at different R_u.

4. Conclusions

Bimodal mesoporous spherical TiO_2 photocatalysts with high photocatalytic activity can be prepared by a one-pot hydrothermal method using titanium sulfate as a precursor in the presence of urea. All prepared TiO_2 powders exhibit bimodal pore-size distributions in the mesoporous region: smaller intra-aggregated pores (peak pore diameter at ca. 2 nm) and larger inter-aggregated pores (peak pore diameters at ca. 12.5 nm). R_u has a significant influence on the morphology, microstructure and photocatalytic activity of TiO_2. With increasing R_u, specific surface areas and porosity increase, on the contrary, the crystallite size and relative anatase crystallinity decrease. The photocatalytic activity of the samples first increases with R_u. At R_u = 2.0, the photocatalytic activity of the sample reaches the highest value and is obviously higher than that of P25 due to relative large specific surface areas and good crystallization. With further increasing R_u, the photocatalytic activity decreases. The formation rate of hydroxyl radicals during photocatalysis has a positive correlation with the photocatalytic activity. At R_u = 2.0, the greatest formation rate of hydroxyl radicals is achieved.

Acknowledgements

This work was partially supported by the National Natural Science Foundation of China (50625208, 20773097, 20877061 and 20803055). This work was also financially supported by the National Basic Research Program of China (2007CB613302 and 2009CB939704).

References

[1] M.R. Hoffmann, S.T. Martin, W. Choi, D.W. Bahnemann, Chem. Rev. 95 (1995) 69.
[2] J.H. Park, S. Kim, A.J. Bard, Nano Lett. 6 (2006) 24.
[3] X.Z. Li, F.B. Li, Environ. Sci. Technol. 35 (2001) 2381.
[4] J.G. Yu, W. Liu, H.G. Yu, Cryst. Growth Des. 8 (2008) 930.
[5] J.G. Yu, S.W. Liu, M.H. Zhou, J. Phys. Chem. C 112 (2008) 2050.
[6] J. Lin, P. Liu, M.J. Meziani, L.F. Allard, Y.P. Sun, J. Am. Chem. Soc. 124 (2002) 11514.
[7] V. Chhabra, V. Pillai, B.K. Mishra, A. Moron, D.O. Shah, Langmuir 11 (1995) 3307.
[8] G.J. Soler-Illia, M. Jobbagy, R.J. Candal, A.E. Regazzoni, M.A. Blesa, J. Dispersion Sci. Technol. 19 (1998) 207.
[9] G.J. Soler-Illia, R.J. Candal, A.E. Regazzoni, M.A. Blesa, Chem. Mater. 9 (1997) 184.
[10] J.G. Yu, M.H. Zhou, B. Cheng, H.G. Yu, X.J. Zhao, J. Mol. Catal. A 227 (2005) 75.
[11] J.G. Yu, M.H. Zhou, B. Cheng, X.J. Zhao, J. Mol. Catal. A 246 (2006) 176.
[12] K. Ishibashi, A. Fujishima, T. Watanabe, K. Hashimoto, Electrochem. Commun. 2 (2000) 207.
[13] J.G. Yu, W.G. Wang, B. Cheng, B.L. Su, J. Phys. Chem. C 113 (2009) 6743.
[14] J.G. Yu, J.C. Yu, M.K.P. Lenug, W. Ho, B. Cheng, X.J. Zhao, J.C. Zhao, J. Catal. 217 (2003) 69.
[15] M.H. Zhou, J.G. Yu, B. Cheng, H.G. Yu, Mater. Chem. Phys. 93 (2005) 159.
[16] A. Fernandez, G. Lassaletta, V.M. Jimenez, A. Justo, A.R. Gonzalez-Elipe, J.M. Herrmann, H. Tahiri, Y. Ait-Ichou, Appl. Catal. B 7 (1995) 49.
[17] M.H. Zhou, J.G. Yu, S.W. Liu, P.C. Zhai, B.B. Huang, Appl. Catal. B 89 (2009) 160.
[18] J.G. Yu, J.F. Xiong, B. Cheng, S.W. Liu, Appl. Catal. B 60 (2005) 211.
[19] J.G. Yu, G.H. Wang, B. Cheng, M.H. Zhou, Appl. Catal. B 69 (2007) 171.
[20] R. Wu, Y. Wei, Y. Zhang, Mater. Res. Bull. 34 (1999) 2131.
[21] H. Wang, J. Miao, J. Zhu, H. Ma, J. Zhu, H. Chen, Langmuir 20 (2004) 11738.
[22] S. Banerjee, A. Santhanam, A. Dhathathreyan, P.M. Rao, Langmuir 19 (2003) 5522.
[23] R. Zanella, L. Delannoy, C. Louis, Appl. Catal. A 291 (2005) 62.
[24] J. Subrt, V. Stengl, S. Bakardjieva, L. Szatmary, Powder Technol. 169 (2006) 33.
[25] E.P. Barrett, L.G. Joyner, P.H. Halenda, J. Am. Chem. Soc. 73 (1951) 373.
[26] N. Kallay, S. Zalac, G. Stefanic, Langmuir 9 (1993) 3457.

[27] M. Ksibi, S. Rossignol, J.M. Tatibouët, C. Trapalis, Mater. Lett. 62 (2008) 4204.
[28] K.S.W. Sing, D.H. Everett, R.A.W. Haul, L. Moscou, R.A. Pierotti, J. Rouquerol, T. Siemieniewska, Pure Appl. Chem. 57 (1985) 603.
[29] A.K. Collins, G.M. Makrigiorgos, G.K. Svensson, Med. Phys. 21 (1994) 1741.
[30] H.M. Khan, M. Anwar, G. Ahmad, J. Radioanal. Nucl. Chem. Lett. 200 (1995) 521.
[31] R.W. Matthews, Radiat. Res. 83 (1980) 27.
[32] S.C. Ashawa, U.R. Kini, U. Madhvanath, Int. J. Appl. Radiat. Isot. 30 (1979) 7.
[33] W.A. Armstrong, R.A. Facey, D.W. Grant, W.G. Humphreys, Can. J. Chem. 41 (1963) 1575.
[34] G.J. Price, E.J. Lenz, Ultrasonics 31 (1993) 451.
[35] G.M. Makrigiorgos, J. Baranowska-Kortylewicz, E. Bump, S.K. Sahu, R.M. Berman, A.I. Kassis, Int. J. Radiat. Biol. 63 (1993) 445.
[36] X. Fang, G. Mark, C. Sonntag, Ultrason. Sonochem. 3 (1996) 57.
[37] J.G. Yu, H.G. Yu, H.T. Guo, M. Li, S. Mann, Small 4 (2008) 87.
[38] J.G. Yu, S.W. Liu, H.G. Yu, J. Catal. 249 (2007) 59.
[39] K.N.P. Kumar, J. Kumar, K. Keizer, J. Am. Ceram. Soc. 77 (1994) 1396.
[40] O. Carp, C.L. Huisman, A. Reller, Prog. Solid State Chem. 32 (2004) 33.
[41] K. Tanaka, M.F.V. Capule, T. Hisanaga, Chem. Phys. Lett. 187 (1991) 73.
[42] M. Anpo, T. Shima, S. Kodama, Y. Kubokawa, J. Phys. Chem. 91 (1987) 4305.
[43] C. Kormann, D.W. Bahnemann, M.R. Hoffmann, J. Phys. Chem. 92 (1988) 5196.
[44] G. Rothenberger, J. Moser, M. Graetzel, N. Serpone, D.K. Sharma, J. Am. Chem. Soc. 107 (1985) 8054.
[45] Q.Y. Li, L. Chen, G.X. Lu, J. Phys. Chem. C 111 (2007) 11494.
[46] J.G. Yu, Y.R. Su, B. Cheng, Adv. Funct. Mater. 17 (2007) 1984.
[47] M.H. Zhou, J.G. Yu, B. Cheng, J. Hazard. Mater. 137 (2006) 1838.